Rapid surface oxidation of Sb_2Te_3 as evidence for a universal trend in the chemical reactivity of tetradymite topological insulators

Andrey A. Volykhov[1,2], Jaime Sánchez-Barriga [3], Anna P. Sirotina[4], Vera S. Neudachina[1], Alexander Frolov[1], Evgeny A. Gerber[1], Elmar Yu. Kataev[1], Boris Senkovsky[5], Nickolay O. Khmelevsky[6], Anatoly A. Aksenenko[6], Natalia V. Korobova[6], Axel Knop-Gericke[7], Oliver Rader[3], Lada V. Yashina[1]

[1] Department of Chemistry, Lomonosov Moscow State University, Leninskie Gory 1/3, 119991 Moscow, Russia

[2] Kurnakov Institute of General and Inorganic Chemistry RAS, Leninskii prosp. 31, 119991 Moscow, Russia

[3] Helmholtz-Zentrum Berlin für Materialien und Energie, Albert-Einstein-Strasse 15, 12489 Berlin, Germany

[4] OAO Giredmet, Bol'shoi Tolmachevskii per. 5/1, 119017 Moscow, Russia

[5] Universität zu Köln, Zülpicher Strasse 77, 50937 Köln, Germany

[6] Moscow State University of Technology STANKIN, Vadkovsky per. 1, 127994 Moscow, Russia

[7] Department of Inorganic Chemistry, Fritz Haber Institute of the Max Planck Society, Faradayweg 4-6, 14195, Berlin, Germany

Abstract

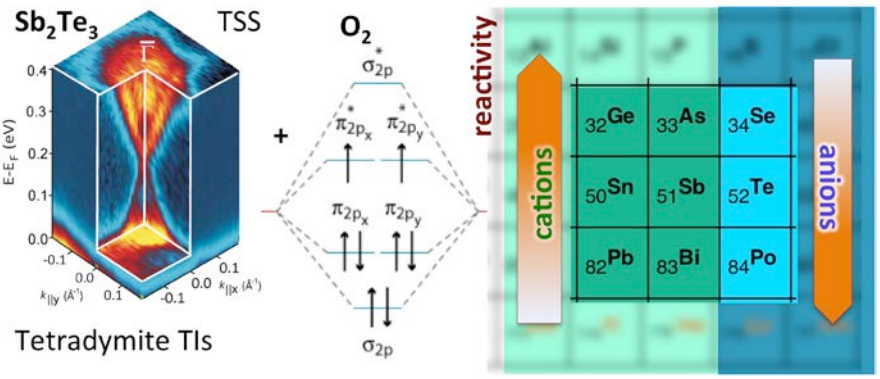

Within the last few years topological insulators (TIs) have attracted a lot of interest due to their unique electronic structure with spin-polarized topological surface states (TSSs), which may pave the way for these materials to have a great potential in multiple applications. However, to enable consideration of TIs as building blocks for novel devices, stability of TSSs towards oxidation should be tested. Among the family of TIs with tetradymite structure, Sb_2Te_3 is of *p*-type and appears to be the least explored material since its TSS is unoccupied in the ground state, a property that allows the use of optical excitations to generate spin currents relevant for spintronics. Here, we report relatively fast surface oxidation of Sb_2Te_3 under ambient conditions. We show that the clean surface reacts rapidly with molecular oxygen and slowly with water, and that humidity plays an important role at the stage of the oxide-layer growth. In humid air, we show that Sb_2Te_3 oxidizes in a time scale of minutes to hours, and much faster than other tetradymite TIs. The high surface reactivity revealed by our experiments is of critical importance and must be taken into account for the production and exploitation of novel TI-based devices using Sb_2Te_3 as working material. Our results provide a fundamental and comprehensive understanding of the universal trend underlying the chemical reactivity of TIs.

Introduction

Topological insulators (TIs) are a nontrivial class of matter that behaves as insulating in the bulk and conducting at the surface[1]. The surface conductivity arises from the fact that strong spin-orbit coupling renders the inversion between the bulk conduction and valence bands, thereby giving rise to spin-polarized topological surface states (TSSs) possessing a unique linear dispersion characteristic of massless particles[1-10].

As opposed to the prototypical TIs Bi_2Se_3 and Bi_2Te_3, which are often referred to as the second generation TIs, Sb_2Te_3 is the only binary tetradymite compound that exhibits exclusively *p*-type doping regardless of the growth method and preparation conditions[11] due to the fact that the equilibrium stability range is fully shifted to Sb side and does not include stoichiometric Sb_2Te_3[12], so that its TSS lies above the Fermi level[13,14]. For this reason, the TSS is always unoccupied in the ground state and can be revealed by ultrafast optical excitation, which in turn has been used to establish the TSS of Sb_2Te_3 as a unique channel for the generation and control of transient spin currents that are of importance for spintronics[15]. Moreover, due to its *p*-doping, interfacing or alloying Sb_2Te_3 with other prototypical TIs such as Bi_2Te_3 has been proposed as one of the promising routes to develop stable topological *p-n* junctions useful for device applications[16]. In fact, such *p-n* junctions might serve as the basis of future optoelectronics, as they are expected to host single gapless chiral edge states localized along the *p-n* interface that can be controlled by external gating or applied magnetic fields[17].

In contrast to both Shockley and Tamm surface states, TSSs are expected to be quite resistant to surface reactions as long as the bulk atomic structure remains intact. However, for surface device applications, detailed knowledge of the stability limits of the surface properties and the behavior of the TSS under ambient conditions are required, especially as preparation techniques of TIs are being extended towards ultrathin freestanding layers[18], nanocrystals[19], nanowires and nanotubes[20], step edges[21] or patterning by lithography[22]. In a context that is much closer to applications and despite of multiple attempts to estimate the reactivity of the prototypical TIs [23-26], many open issues remain. While the time scale for Bi_2Te_3 oxidation in wet air is well characterized[8], for Bi_2Se_3 and $Bi_2(Se,Te)_3$ the situation is much less clear. The available data scatter significantly from negligible reactivity to rapid oxidation[23,24]. Although the naturally perfect crystal surface is basically robust towards oxidation, for low-dimensional structures of the same material the formation of an oxide layer is usually observed[27]. Certain contradiction exists in the explanation of such a difference. On the one hand, Thomas and co-workers found by means of photoelectron microscopy that step-edges oxidize first[24], thus promoting further

proliferation of the oxide layer. The density of step-edges is particularly high for films grown by molecular beam epitaxy (MBE), which indeed oxidize even faster[23]. Moreover, nanoscale mapping under ambient conditions reveals a 10−100x current enhancement at step-edges as compared to that on terraces[25]. On the other hand, scanning probe microscopy data evidence very similar behavior in the absence of morphology features upon oxidation, resulting in the formation of a flat and uniform oxide layer[23,26].

Our previous systematic photoemission studies of the prototypical TIs Bi_2Se_3 and Bi_2Te_3, as well as density-functional theory (DFT) calculations, revealed that both O_2 and H_2O adsorb molecularly[23]. In particular, only simultaneous adsorption of oxygen and water molecules was shown to give rise to a surface reaction in the case of Bi_2Te_3. This reaction included two crucial steps: (1) surface termination with hydroxyl groups attached to the Te atoms, and (2) formation of oxide species with oxygen bonded to both Bi and Te atoms. For Bi_2Se_3 crystals of equally high perfection, these processes were not detected after long exposures to air, so that high resistance against oxidation was observed instead. To completely understand the origin of the different oxidation behaviour, and whether there is a systematic trend underlying the chemical reactivity of TIs, it is absolutely necessary to obtain the corresponding information on the reactivity of Sb_2Te_3. A possible scenario, where step-edges or other imperfections of the crystal do not play a substantial role, is that the reactivity towards oxygen increases for lighter cations and heavier anions, so that substitution of Se by Te or Bi by Sb leads to a remarkable increase of the oxidation rate. However, up to now information concerning the surface reactivity of Sb_2Te_3 that would shed light on this issue is missing. Taking into account the general trend observed for other chalcogenide compounds (IV-VI, II-VI)[28], this raises questions regarding the surface stability of Sb_2Te_3 as compared to the one of Bi_2Te_3, and whether a similar trend not yet confirmed experimentally exists in the case of TIs.

To resolve this issue, in the present work we investigate the reactivity of Sb_2Te_3 using photoelectron spectroscopy in a wide range of experimental conditions, including air humidity, and oxygen pressure (up to 20 mbar). Additionally, we provide a detailed understanding of the outcome of experiments under constant pressure of vapour and liquid water. Our results demonstrate a much faster oxidation of Sb_2Te_3 in ambient air as compared to any other prototypical TI, and supply a clear evidence of the underlying physical and chemical phenomenon yielding higher surface reactivity. The reaction mechanism is further revealed by combining the experimental data with the results of DFT calculations. Our work reveals a universal trend in the chemical reactivity of tetradymite TIs and serves as a benchmark for the

understanding of oxidation processes in more complex families of layered TIs, providing a criterion for optimizing and manufacturing stable TI-based nanodevices for future applications.

Results and discussion

Clean Sb_2Te_3 (111) surfaces were obtained by cleaving a single crystal (Figs. 1a-c) along the Van der Waals gap (Fig. 1d). The typical cleavage morphology includes low density of steps (few per micron) as revealed by atomic force microscopy (AFM) in Fig. 1e. Due to the strong *p*-doping of the crystal, the TSS of Sb_2Te_3 is located above the Fermi level, thus it is not possible to observe it using conventional angle-resolved photoemission spectroscopy (ARPES). Therefore, we combined a pump-probe laser scheme with ARPES to excite electrons above the Fermi level using 1.5 eV photons and detect the excited electrons using 6 eV photons, allowing us to monitor the electronic band structure above the Fermi level. The obtained energy-momentum dispersion of the TSS around the $\bar{\Gamma}$ point of the surface Brillouin zone is depicted in Fig. 1f.

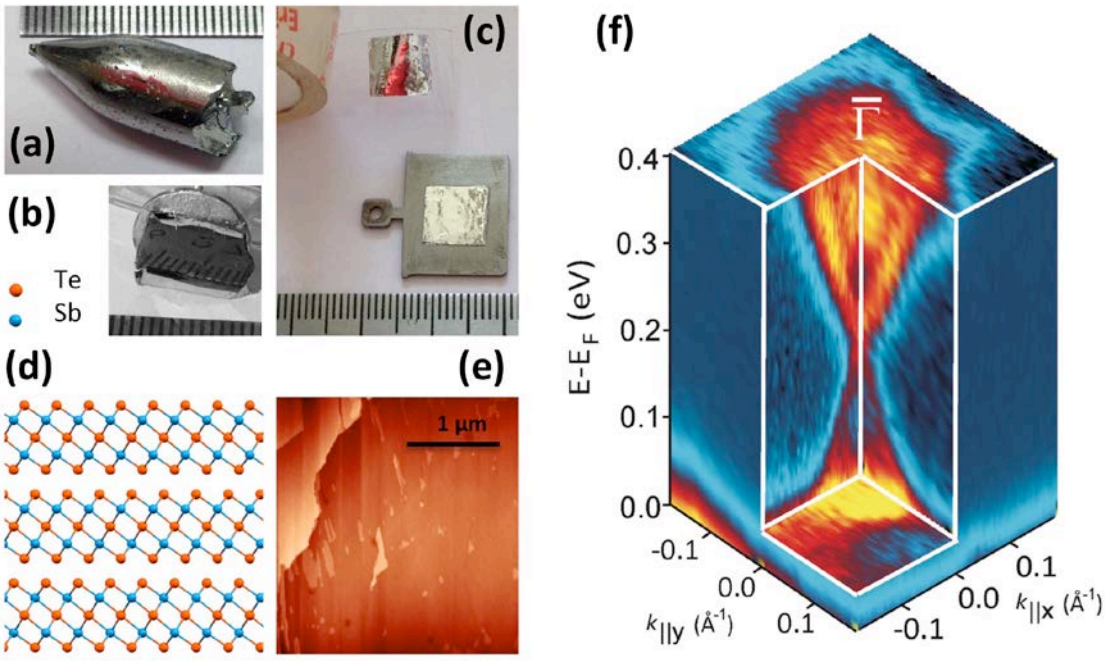

Fig. 1. A photograph of the Sb_2Te_3 crystal (a), sample (b), and an illustration of surface preparation using scotch tape (c), d) crystal structure, e) an atomic force microscopy image revealing low density of step-edges, f) energy-momentum dispersion of the TSS for Sb_2Te_3 above the Fermi level (E_F) obtained around the $\bar{\Gamma}$ point of the surface Brillouin zone using pump-probe ARPES. The linear dispersion of the Dirac cone is clearly resolved, with an additional intensity contribution from the bulk-conduction and valence bands at 0.3 eV and 0.05 eV, respectively.

Here, we clearly observe the TSS linear dispersion characteristic of Dirac fermions, with the Dirac node located at ~0.25 eV above the Fermi level. The sharp and intense features confirm the

high quality of the surface. Moreover, distinct contributions from the bulk-conduction band (BCB) and valence band states (BVB) are also observed. In these regions, it is seen how the TSS bands at opposite momenta merge with the bulk bands bridging the gap of the volume, one of the unique properties of TIs. Such prepared and characterized Sb_2Te_3 surfaces were probed by x-ray photoelectron spectroscopy (XPS) after well-defined exposures to air with different relative humidity (*ex situ*), oxygen (*ex situ*), water vapours (*in situ*), or gas-free liquid water (*ex situ*). To provide the ultimate surface sensitivity and spectral resolution, Sb 4*d* and Te 4*d* core-level spectra were recorded at the photoelectron kinetic energies of 50, 75 or 100 eV.

First we discuss the results of the reactions occurring at the surface in atmospheric air. The spectra obtained for the clean surface upon cleavage in ultrahigh vacuum (UHV) and after different exposures to air are shown in Fig. 2a. For the clean surface, both Sb 4*d* and Te 4*d* are single-component doublets. After a certain air exposure (here being equal to 2 h) a relatively thick oxide layer forms, corresponding to an oxidized single quintuple layer (QL), which is confirmed by the typical multicomponent spectra. In the Te 5*d* spectrum, the Te IV component shifted by 3.80 eV from the initial Te I peak corresponds to the formal oxidation state +4[29]. Other two components, Te II (shifted by 0.6 eV) and Te III (shifted by 1.2 eV), exhibit an intensity maximum at binding energies close to those of neutral Te. In the Sb 4*d* spectrum, the Sb II feature split by 1.38 eV from the initial peak corresponds to the formation of more ionic Sb-O bonds in the Sb-O-Te fragment with the same formal Sb oxidation state +3. We also measured O 1*s* photoemission spectra at high kinetic energies (see Supplemental information) in which we observe single component located at 530.6 eV that is related to the formation of oxide-type bonds. This value quantitatively agrees with the O 1*s* binding energy corresponding to Sb_2O_3[30].

It should be emphasized that, in the course of multiple experiments, due to the fast surface oxidation we have never observed any intermediate state between the clean and strongly oxidized one (see Fig.2a). Moreover, the exact time period corresponding to the appearance of the surface oxide layer cannot be determined unambiguously for all samples as it is subject to variations of statistical nature. We have taken special care to control the oxidation state of the sample by avoiding any possible influence of humidity and temperature variations, or any effect of storage under UHV conditions. However, these precautions did not allow us to completely suppress the scattering in the data, which nevertheless show a clear tendency as a function of oxidation time (see Figs. 2b and 2c). In addition, we observed that the oxidation occurs non-uniformly over the surface in a length scale of several millimeters. This behavior raises the question of what is the mechanism underlying the fast surface oxidation observed in our

experiments, which we discuss below.

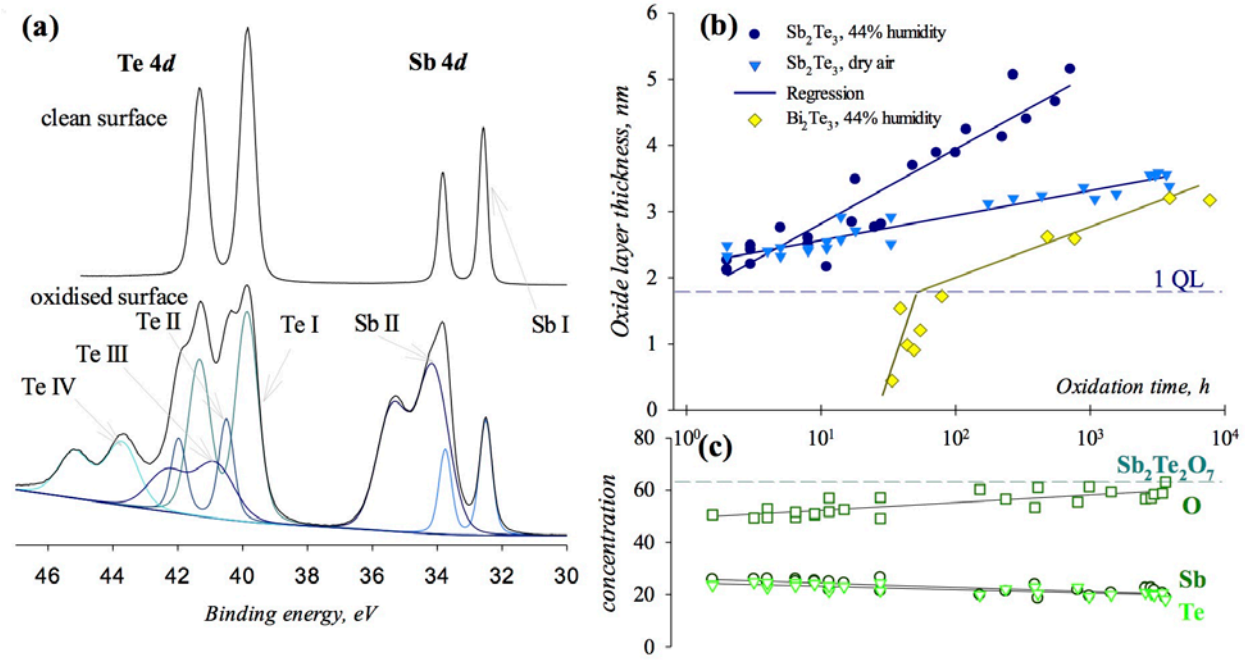

Fig. 2. Air exposure of Sb_2Te_3 at 298±2 K: a) High resolution photoemission spectra for the Sb_2Te_3 (111) clean surface and surfaces exposed to humid (44%) air during 1 and 2 h, the photon energy is 125 eV; b) the oxidation kinetics for the Sb_2Te_3 (111) surface at 298 K: time dependence of the oxide layer thickness for oxidation in dry and wet air at humidity of 44%. The spectra were recorded using a monochromatic Al K_α source. Bi_2Te_3 data were added for comparison, c) time dependence of the oxide layer composition.

The fast oxidation observed in the present work distinguishes Sb_2Te_3 from Bi_2Te_3, and Bi_2Se_3, which we studied earlier[23]. Generally, the oxidation proceeds in several steps, which are:

(i) Molecular adsorption and induction period;

(ii) Surface reaction and oxidation of the first layer;

(iii) In-depth oxidation with long-term kinetics.

The statistical nature of the oxidation time observed in the case of Sb_2Te_3 can be explained by a combination of a relatively slow step (i), i.e. a long induction period, and a very fast step (ii). As the induction period is of statistical nature (from minutes to hours), and it is followed by fast oxidation of the first QL, their combination gives rise to additional scattering in the data related to the exposure time from 15 min to 14 h (for further details, please see Fig. S1 of the Supplementary Information). One can assume that surface defects like steps, might play a role to overcome the energy threshold for oxidation. Since the steps are of very low density at the surface, the oxidation threshold can be expected to be slightly sensitive to variations in the

number of steps. Although these variations might introduce some additional source of scattering in the data presented for different humidity values in Fig. 2b, the overall behavior of the data strongly indicates that water vapours do not play an essential role in steps (i) and (ii).

In fact, the results presented in Fig. 2b allow us to visualize the complete oxidation kinetics. Here, the data for Sb_2Te_3 are presented with respect to the time-dependent variation of the oxide layer thickness and calculated from the Te 3*d* core level spectra using the Hill equation (for further details on the layer thickness please see Supplementary Information). For comparison, we also show the Bi_2Te_3 oxidation kinetics. Very clearly, for the Sb_2Te_3 (111) surface the oxide layer thickness increases linearly as a function of oxidation time, while no data points are available for an oxide layer thickness below 1 nm. At the same time, for the Bi_2Te_3 (111) surface the kinetics exhibits two distinct steps, which are associated to steps (ii) and (iii). Therefore, step (ii) is much faster for Sb_2Te_3 than that for Bi_2Te_3 and not resolvable experimentally. It should be also noted that the oxide layer appears to be enriched in antimony, so that the Sb to Te atomic ratio is about 1 to 1 and does not change upon further oxidation. The oxygen content constantly increases until the ultimate stoichiometry of the oxide layer $Sb_2Te_2O_7$ is obtained, where tellurium is totally converted to Te^{4+}. The oxide layer composition is given in Fig. 2c.

The kinetics of the oxide layer growth for Sb_2Te_3 appears to be different for high and humid air. The oxidation rate in dry air is generally lower as compared to that obtained at a relatively low humidity of 44%. This fact pinpoints the active role of water vapour in the oxidation during step (iii).

To gain further insight into this behavior we studied water adsorption on the Sb_2Te_3 (111) surface *in situ* using near-ambient pressure XPS (NAP XPS), which is established as a powerful tool to probe surface reactions that indeed can be rather different from those for surfaces in vacuum. For this reason, we performed an experiment at a partial water pressure of $P(H_2O) = 0.10$ mbar during a period of 10 h. The results are depicted in Fig. 3 and compared to results for Bi_2Te_3 obtained previously[23]. It should be emphasized that the Sb_2Te_3 (111) surface is well wettable with water; therefore, large-drop formation at the surface during *in situ* experiments is obviously excluded, meaning that we probe reliably the water-crystal interface. During the whole period of measurements the water layer thickness progressively increases at the surface up to 5 nm, while no modification of the Sb 3*d* and Te 3*d* core level spectra is observed. This result evidences that the Sb_2Te_3 surface does not directly react with water under the given experimental conditions. The O 1*s* peak can be treated as a single broad component positioned at a binding energy slightly increasing with time from 532.8 eV to 533.2 eV, as measured relative to Sb $3d_{5/2}$,

which is assigned to physically adsorbed water. This tiny effect on the binding energy can be attributed to H-bond formation accompanying water condensation at the surface. Therefore, one can conclude that water does not react chemically with the surface at $P(H_2O) = 0.10$ mbar at least during 10 h. The water adsorption is faster for Sb_2Te_3 than for Bi_2Te_3 thus indicating the stronger interaction between water and the former.

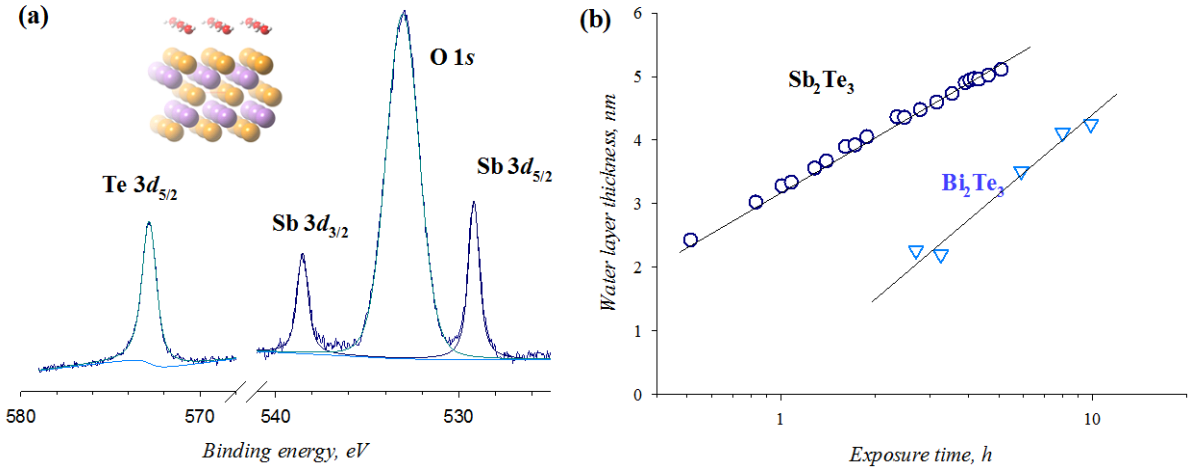

Fig. 3. Molecular adsorption of water vapour at the Sb_2Te_3 (111) surface measured at 0.1 mbar and 298±2 K, excitation energy 200 eV: a) Te 3*d*, Sb 3*d*, and O 1*s* spectra. The inset shows the most beneficial structure modeling the molecular absorption of water. Yellow, violet, red and gray colors depict Te, Sb, O and H atoms, respectively. b) kinetics of the water layer growth estimated using the Hill equation.

Our theoretical investigation of the water molecule adsorption reveals that the on-top position is more beneficial, by almost 2 eV, than the hollow one. The most stable structure is depicted in Fig. 3a as an inset. The on-top structures are characterized by negligible chemical shifts both for Sb 3*d* and Te 3*d* core levels. In all cases including hollow water molecule displacement new chemical bonds are not formed between Sb_2Te_3 and H_2O. To understand this issue from the opposite side of the equilibrium state, we modeled dissociative adsorption structures with Sb-H and Te-OH bonds and, vice versa, with Sb-OH and Te-H bonds. However, all these structures were found to be less stable than those for molecular adsorption. Therefore, our experimental data and theoretical modeling evidence stability of the Sb_2Te_3 (111) surface towards hydrolysis.

We further investigated the reaction with water in its liquid state to provide conditions beneficial for hydrolysis. Water was preliminary degased and maintained under completely air free conditions. After the surface treatment with liquid water, our high-resolution Te 4*d* spectra display a two-component structure with a new component slightly shifted by 0.72 eV eV towards higher binding energy, as it follows from Fig. 4a. Such binding energy corresponds to elemental tellurium. In addition, the surface becomes enriched in tellurium as we found from composition

quantification measurements. Our experiments with Sb_2Te_3 powders washed in degassed water with subsequent chemical analysis of the washwater by inductively coupled plasma - mass spectrometry (ICP-MS) reveal the presence of antimony in amounts proportional to the reaction time (see Fig. 4b). Therefore, we conclude that Sb is leached out from the surface. The time variation of the surface composition is illustrated in Fig. 4b. One can see that the time period of ~10 h corresponds to leaching of the first Sb layer, which results in the structure Te-Te-Sb-Te instead of Te-Sb-Te-Sb-Te for the first QL. We modelled this situation using DFT and the calculated Te 4*d* chemical shift relative to the bulk (+0.45eV) is in reasonable agreement with the experimental one. It should be mentioned that if water is in contact with air the surface oxidation occurs already after 8 h with the corresponding Te^{+4} formation, with the reaction products being similar to those observed in humid air. This behavior is different from Bi_2Te_3, where we observed surface oxidation only after dissolution of some amount of air in degassed liquid water after 1 day of reaction[23]. Sb leaching observed in degassed water proves that Sb_2Te_3 is reactive with water since the Sb-Te bonds break. According to our calculations the reaction with gaseous water is not energetically beneficial. One can suppose that the driving force of Sb leaching is the Sb^{3+} solvation energy. The solvation is hardly possible in a thin layer of water formed as a result of vapor adsorption.

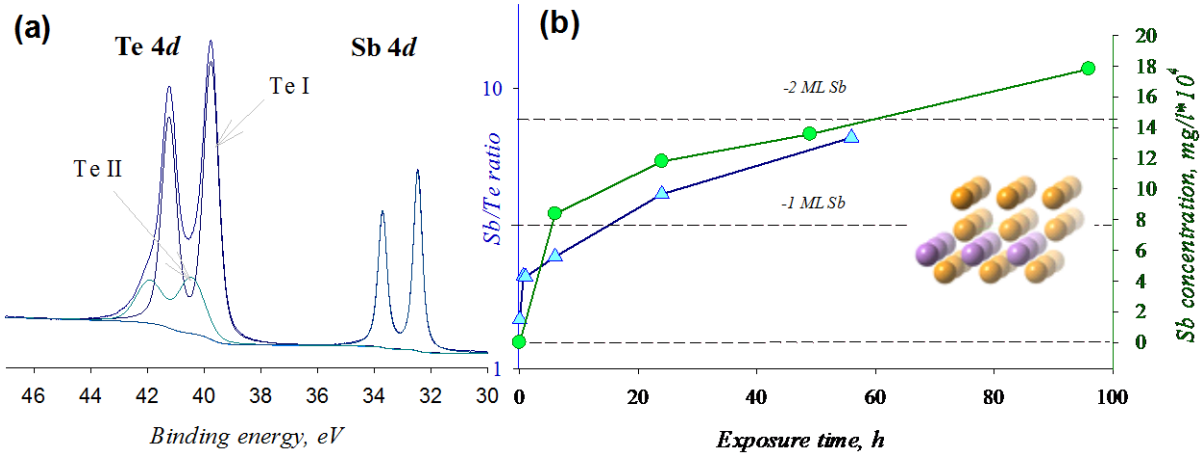

Fig. 4. Sb_2Te_3 hydrolysis: a) A typical high resolution photoemission spectrum for the Sb_2Te_3 (111) surface exposed to liquid water during 6.3 h at 298±2 K, the photon energy is 125 eV; b) Time dependence of the Sb_2Te_3 (111) surface composition (left scale) and Sb concentration in water (right scale). Inset: Modeled structure for a surface depleted in Sb. Yellow and violet colors depict Te and Sb atoms, respectively.

The leaching is relatively slow, it occurs in a time scale of approximately 10 hours. Within the same time period the reaction in humid air gives rise to total modification of the first QL. For this reason the humidity is evidently not important during step (ii). Nevertheless, the Sb_2Te_3 (111) surface manifests rather weak but detectable reactivity with water in its liquid state. Now

we return to the question of possible reactions between Sb_2Te_3 and molecular oxygen. According to our DFT calculations adsorption of an O_2 molecule can result into its dissociation. We have considered four different possible starting geometries. Two of them give rise to O_2 dissociation and Sb-O-Te bond formation as presented in Fig. 5a (left structure). The corresponding formation energy is 3 eV, which is lower than for the structures modeling molecular adsorption. Based on optimized geometries the activation energy of oxygen dissociative adsorption is estimated to be 0.24 eV.

Indeed, being exposed to oxygen, Sb_2Te_3 is oxidized at the partial pressure of 200 mbar already after 30 min, i.e., the behavior is similar to the one in ambient atmosphere. Moreover, the oxidation reaction occurs even at much lower pressures starting from 0.01 mbar, while we did not observe any reaction at $P(O_2) = 8\ 10^{-5}$ mbar. The experimental data on the Sb_2Te_3 oxidation with molecular oxygen are shown in Fig.5b, where the oxide layer thickness is represented as a function of oxygen exposure. Interestingly, the oxidation rate in pure oxygen is statistically even higher than the reaction rate in humid air. The most probable reason is that the adsorption sites are occupied by inert molecules especially adventitious carbon, which is always present at the surface exposed to air.

Both Sb 4*d* and Te 4*d* spectral features appearing upon oxidation in oxygen are of the same nature as ones observed after oxidation in humid air. One can conclude that the reaction products are the same for pure oxygen and humid air therefore water vapours indeed play a minor role during the first stage of oxidation. The modeled structures pinpoint possible mechanisms of oxidation with H_2O participating via hydroxyl groups attached to the surface tellurium atoms (see Supplementary Information for more details). Note that the hydroxyl groups are not present during the oxidation of the Bi_2Te_3 surface, while for Sb_2Te_3 follow the reaction:

$Sb_2Te_3+3/2O_2+3H_2O=Sb_2(Te\text{-}2OH)_3$.

The chemical shifts in the Sb 4*d* and Te 4*d* spectra for the species occurring at the surface are generally in a good agreement with calculated ones if final state effects are properly taken into account. We therefore correct the observed chemical shifts by the difference in relaxation energy estimated experimentally using the Auger parameter concept[31]. After this correction, we compared the resulting experimental initial state chemical shifts to the calculated ones. For Sb cation atoms, the final state effect in Sb 4*d* spectra is rather large and estimated to be about 1 eV, therefore, the experimentally observed chemical shift is mostly due to a final state effect. For the Te anion atoms, the final state effect is negligible. Te 4*d* chemical shift depends strongly on the number of O atoms attached to the given Te atom. The structures corresponding to the spectral

features are highlighted in Fig. 5c. In addition, the angular dependence of the ratio from different spectral components (see Supplementary Information) reveals that the Te III component corresponds to the state at the very surface revealing its intermediate nature. The Te II feature is

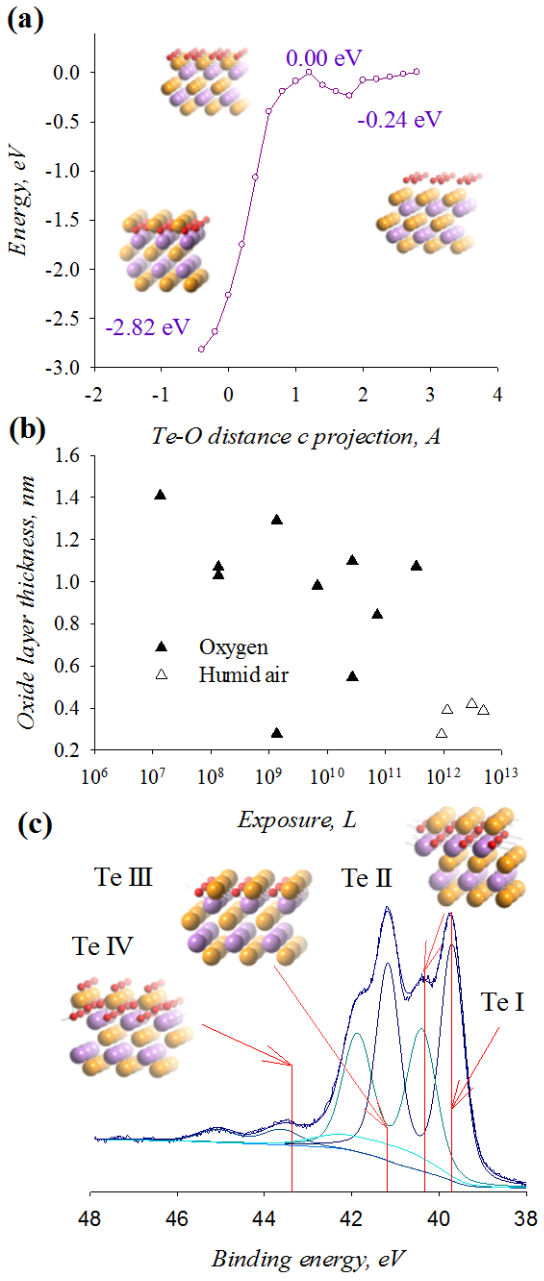

Fig. 5. O_2 pathway at the Sb_2Te_3 (111) surface. (a) Activation barrier for dissociative adsorption with corresponding structures, where zero distance means the Te atoms surface plane. (b) Oxide layer thickness obtained at different exposures. (c) Typical Te 4*d* spectrum with spectral component assignment to the specific geometries. In all modeled structures yellow, violet and red colors depict Te, Sb and O atoms, respectively.

most probably present at the interface oxide layer and crystal bulk. AFM measurements indicate that the surface morphology is preserved after air exposure therefore the oxide is formed as a layer uniform in thickness. It should be also noted that we would expect one more air

constituent, CO_2, to play an essential role in the surface degradation. However, we have never observed carbonate-related species on the air- exposed surfaces in our experiments. Therefore, we may conclude that CO_2 plays no role in the surface degradation.

Our results for Sb_2Te_3 demonstrate much faster chemical degradation in atmospheric air than Bi_2Te_3 and especially Bi_2Se_3, with the atomic mechanism being different. Sb_2Te_3 reacts with oxygen and water separately. Air oxidation includes the reaction with molecular oxygen; water plays negligible role at the beginning of the process and makes notable contribution in oxide layer growth kinetics. The higher reactivity of Sb_2Te_3 is in line with the trends for binary semiconductors such as IV-VI compounds[28], where it increases for heavier anions and lighter cations as we found experimentally and theoretically in the present work. The main reason for rapid oxidation of Sb_2Te_3 is chemical and higher energy benefit for the formation of Sb-O-Te bonds than Bi-O-Te bonds.

Our mechanistic studies on the Sb_2Te_3 oxidation behavior sheds light on the problem of reactivity of Bi_2Se_3 for which completely different results have been reported[23-27]. By analogy with Sb_2Te_3 the scattering and differences between the published experimental data can be attributed to the fact that the induction period is huge due to the low probability of the elementary chemical reaction event, which occurs on a time scale comparable with or faster than the time scale of experimental exposures. Under these circumstances, surface defects might play a role even if the density of defects is low. As a result, the oxidation time scale cannot be determined unambiguously, as from sample to sample, it is of statistical nature.

The reactivity of Sb_2Te_3 is still much lower than the one of many compound semiconductors and topological crystalline insulators, like Sn-Te, Pb-Sn-Te or Pb-Sn-Se due to the layered structure and the absence of dangling bonds at the surface. Moreover, the formation of an oxide layer itself does not destroy the TSS, which is still present at the buried oxide-TI interface, even if oxide layer thickness is large. Control of the oxidation process is rather critical either for low dimensional structures where the band structure strongly depends on the number of QLs, or for the case when surface rather than interface properties are used or investigated.

Conclusions

To summarize, we have shown that the prototypical topological insulator Sb_2Te_3 degrades much faster than Bi_2Te_3 and especially than Bi_2Se_3 under ambient conditions. For Bi_2Te_3, the oxidation kinetics has two distinct steps, with the first step corresponding to a total conversion of the first quintuple layer in oxide. In contrast, the first oxidation step in Sb_2Te_3 is found to be remarkably

fast. The oxidation is even faster in the presence of water vapours, although there is no reaction with gaseous water itself at pressures around 0.1 mBar, as it follows from *in situ* studies by NAP XPS. We have demonstrated that Sb_2Te_3 shows notable reactivity towards liquid water producing Te-enriched surface due to Sb leaching. The relatively high-surface reactivity observed in the present work evidences a universal trend in the chemical reactivity of tetradymite TIs, which increases for heavier anions and lighter cations. Our work serves as a benchmark for the understanding of oxidation processes in more complex families of layered TIs, providing a criterion for optimizing the stability of future TI-based nanodevices under ambient conditions.

Methods

Sb_2Te_3 single crystals were grown by the Bridgman method. Bulk single crystals were cleaved *in situ* for ARPES and near ambient pressure (NAP) XPS experiments or *ex situ* for the photoemission studies of oxidation at high exposures. The high quality of the achieved (111) surfaces was verified by low-energy electron diffraction (LEED), the presence of sharp features from the topological surface states and the valence band in the ARPES dispersions. Pump-probe ARPES experiments were performed at room temperature using the first (1.5 eV) and fourth (6 eV) harmonics of a homemade fs-laser system coupled to an ultrafast amplifier operating at 100 kHz repetition rate. Photoelectrons were detected with a Scienta R4000 hemispherical analyzer, and the angular and energy resolutions were 0.3° and 30 meV, respectively.

Core-level photoemission studies were carried out using several facilities of Helmholtz-Zentrum Berlin, Germany. The NAP XPS data were obtained at the ISISS beamline equipped with a SPECS Phoibos 150 analyzer under water pressures of ~0.1 mbar. The Sb 3*d*, Te 3*d* and O 1*s* spectra were recorded at different kinetic energies between 200 and 800 eV to provide variable surface sensitivity.

For *ex situ* experiments, freshly cleaved surfaces were exposed for defined periods of time to dried or humid air or washed in water at 1 bar and 2098 K. The Sb 4d, Te 4d and O 1s spectra were recorded with high surface sensitivity (at the same electron kinetic energy 50, 75 or 100 eV) at the Russian German beamline. The XPS spectra acquisition was performed using a SPECS Phoibos 150 electron energy analyzer at variable detection angles.

The long-term oxidation kinetics was studied using an Axis Ultra DLD (Kratos) and a *K*-alpha (Thermo Fisher Scientific) spectrometer, both equipped with monochromatic Al K_α sources. All XPS spectra were fitted by Gaussian/Lorentzian convolution functions with simultaneous optimization of the background parameters. The background was modelled using a combination

of a Shirley and a Tougaard background.

Theoretical modelling of the surface reactions was performed within the DFT approach using the PW-GGA method (VASP code)[32-34]. Lattice constants were fixed, while positions of all atoms were varied. Core-level shifts were calculated in the initial-state approximation as the variation of electrostatic potentials at the atomic centers after adsorption.

Acknowledgements

Financial support from the Russian Foundation for Basic Research, the Russian-German Laboratory at BESSY II and the Deutsche Forschungsgemeinschaft (DFG Grant No. SPP 1666) is gratefully acknowledged. We thank Helmholtz-Zentrum Berlin for the allocation of synchrotron radiation beamtimes at RGBL and ISISS beamlines and the Supercomputing Center of the Lomonosov Moscow State University for providing access to supercomputers. The authors thank Daria Tsukanova, Alina Belova and Tatiana Zakharchenko for technical support.

References

[1] Hasan, M. Z.; Kane, C. L. *Colloquium* : Topological Insulators. *Rev. Mod. Phys.* **2010**, *82*, 3045–3067.

[2] Kane, C. L.; Mele, E. J. Z2 Topological Order and the Quantum Spin Hall Effect. *Phys. Rev. Lett.* **2005**, *95*, 146802.

[3] Li, R.; Wang, J.; Qi, X.-L.; Zhang, S.-C. Dynamical Axion Field in Topological Magnetic Insulators. *Nat. Phys.* **2010**, *6*, 284–288.

[4] Essin, A. M.; Moore, J. E.; Vanderbilt, D. Magnetoelectric Polarizability and Axion Electrodynamics in Crystalline Insulators. *Phys. Rev. Lett.* **2009**, *102*, 146805.

[5] Roy, R. Topological Phases and the Quantum Spin Hall Effect in Three Dimensions. *Phys. Rev. B* **2009**, *79*, 195322.

[6] Qi, X.-L.; Li, R.; Zang, J.; Zhang, S.-C. Inducing a Magnetic Monopole with Topological Surface States. *Science* **2009**, *323*, 1184–1187.

[7] Fu, L.; Kane, C. L.; Mele, E. J. Topological Insulators in Three Dimensions. *Phys. Rev. Lett.* **2007**, *98*, 106803.

[8] Moore, J. E.; Balents, L. Topological Invariants of Time-Reversal-Invariant Band Structures. *Phys. Rev. B* **2007**, *75*, 121306(R).

[9] Shuichi Murakami. Phase Transition between the Quantum Spin Hall and Insulator Phases in 3D: Emergence of a Topological Gapless Phase. *New J. Phys.* **2007**, *9*, 356–356.

[10] Sánchez-Barriga, J ; Varykhalov, A. ; Braun, J. ; Xu, S. -Y. ; Alidoust, N. ; Kornilov, O.; Minár, J. ; Hummer, K. ; Springholz, G. ; Bauer, G.; Schumann, R.; Yashina, L. V.; Ebert, H.; Hasan, M. Z.; Rader, O. Photoemission of Bi_2Se_3 with Circularly Polarized Light: Probe of Spin Polarization or Means for Spin Manipulation?. *Phys. Rev. X* **2014**, *4*, 011046.

[11] Takagaki, Y.; Giussani, A.; Tominaga, J.; Jahn, U.; Calarco, R. Transport Properties in a Sb–Te Binary Topological-Insulator System. *J. Phys. Condens. Matter* **2013**, *25*, 345801.

[12] Ghosh, G. The Sb-Te (antimony-Tellurium) System. *J. Phase Equilibria* **1994**, *15*, 349–360.

[13] Seibel, C.; Bentmann, H.; Braun, J.; Minár, J.; Maaß, H.; Sakamoto, K.; Arita, M.; Shimada, K.; Ebert, H.; Reinert, F. Connection of a Topological Surface State with the Bulk Continuum in Sb_2Te_3 (0001). *Phys. Rev. Lett.* **2015**, *114*, 066802.

[14] Pauly, C.; Bihlmayer, G.; Liebmann, M.; Grob, M.; Georgi, A.; Subramaniam, D.; Scholz, M. R.; Sánchez-Barriga, J.; Varykhalov, A.; Blügel, S.; Rader, O.; Morgenstern, M. Probing Two Topological Surface Bands of Sb 2 Te 3 by Spin-Polarized Photoemission Spectroscopy. *Phys. Rev. B* **2012**, *86*, 235106.

[15] Sánchez-Barriga, J. ; Golias, E. ; Varykhalov, A.; Braun, J. ; Yashina, L. V. ; Schumann, R. ; Minár, J.; Ebert, H.; Kornilov, O. ; Rader, O. Ultrafast spin-polarization control of Dirac fermions in topological insulators. *Phys. Rev. B* **2016**, *93*, 155426.

[16] Eschbach, M. *et al.* Realization of a vertical topological p–n junction in epitaxial Sb_2Te_3/Bi_2Te_3 heterostructures. *Nat. Commun.* **2015**, *6*, 8816.

[17] Wang, J.; Chen, X.; Zhu, B.-F.; Zhang, S-C. Topological p-n junction. *Phys. Rev. B* **2012**, *85*, 235131.

[18] Kim, B. G.; Lim, C.-H.; Choi, S.-M.; Seo, W.-S.; Lee, H.-L.; Hyun, S.-H.; Jeong, S.-M. Free-Standing Bi–Sb–Te Films Derived from Thermal Annealing of Sputter-Deposited Sb_2Te_3 /Bi_2Te_3 Multilayer Films for Thermoelectric Applications. *Cryst. Eng. Comm* **2015**, *17*, 7522–7527.

[19] Zhao, Y.; Burda, C. Chemical Synthesis of $Bi_{0.5}Sb_{1.5}Te_3$ Nanocrystals and Their Surface Oxidation Properties. *ACS Appl. Mater. Interfaces* **2009**, *1*, 1259–1263.

[20] Pinisetty, D.; Gupta, M.; Karki, A. B.; Young, D. P.; Devireddy, R. V. Fabrication and Characterization of Electrodeposited Antimony Telluride Crystalline Nanowires and Nanotubes. *J. Mater. Chem.* **2011**, *21*, 4098–4107.

[21] Sung, J. H.; Heo, H.; Hwang, I.; Lim, M.; Lee, D.; Kang, K.; Choi, H. C.; Park, J.-H.; Jhi, S.-H.; Jo, M.-H. Atomic Layer-by-Layer Thermoelectric Conversion in Topological Insulator Bismuth/Antimony Tellurides. *Nano Lett.* **2014**, *14*, 4030–4035.

[22] Wang, R.; Wei, J.; Fan, Y. Chalcogenide Phase-Change Thin Films Used as Grayscale Photolithography Materials. *Opt. Express* **2014**, *22*, 4973.

[23] Yashina, L. V.; Sánchez-Barriga, J.; Scholz, M. R.; Volykhov, A. A.; Sirotina, A. P.; Neudachina, V., S.; Tamm, M. E.; Varykhalov, A.; Marchenko, D.; Springholz, G.; Bauer, G.; Knop-Gericke, A.; Rader, O. Negligible Surface Reactivity of Topological Insulators Bi_2Se_3 and Bi_2Te_3 towards Oxygen and Water. *ACS Nano* **2013**, *7*, 5181–5191.

[24] Thomas, C. R.; Vallon, M. K.; Frith, M. G.; Sezen, H.; Kushwaha, S. K.; Cava, R. J.; Schwartz, J.; Bernasek, S. L. Surface Oxidation of $Bi_2(Te,Se)_3$ Topological Insulators Depends on Cleavage Accuracy. *Chem. Mater.* **2016**, *28*, 35–39.

[25] Macedo, R. J.; Harrison, S. E.; Dorofeeva, T. S.; Harris, J. S.; Kiehl, R. A. Nanoscale Probing of Local Electrical Characteristics on MBE-Grown Bi_2Te_3 Surfaces under Ambient Conditions. *Nano Lett.* **2015**, *15*, 4241–4247.

[26] Hwang, J. H.; Park, J.; Kwon, S.; Kim, J. S.; Park, J. Y. Role of Oxidation on Surface Conductance of the Topological Insulator Bi_2Te_2Se. *Surf. Sci.* **2014**, *630*, 153–157.

[27] Kong, D. S.; Cha, J. J.; Lai, K. J.; Peng, H. L.; Analytis, J. G.; Meister, S.; Chen, Y. L.; Zhang, H. J.; Fisher, I. R.; Shen, Z. X.*et al.*Rapid Surface Oxidation as a Source of Surface Degradation Factor for Bi_2Se_3, *ACS Nano* **2011**, *5*, 4698– 4703

[28] Volykhov, A. A.; Yashina, L. V.; Zyubina, T. S.; Shtanov, V. I.; Neudachina, V. S.; Püttner, R.; Zyubin, A. S. Comparative Reactivity of AIVBVI Compounds in Their Reactions with Dioxygen. *Russ. J. Inorg. Chem.* **2011**, *56*, 1284–1289.

[29] Yashina, L. V.; Zyubina, T. S.; Püttner, R.; Zyubin, A. S.; Shtanov, V. I.; Tikhonov, E. V. A Combined Photoelectron Spectroscopy and Ab Initio Study of the Adsorbate System O_2 /PbTe(001) and the Oxide Layer Growth Kinetics. *J. Phys. Chem. C* **2008**, *112*, 19995–20006.

[30] Linarez Pérez, O. E.; Sánchez, M. D.; López Teijelo, M. Characterization of growth of anodic antimony oxide films by ellipsometry and XPS. *J. Electroanal. Chem.* **2010,** *645*, 143-148.

[31] Moretti, G. The Auger Parameter and the Polarization Energy: A Simple Electrostatic Model. *Surf. Interface Anal.* **1990**, *16*, 159–162.

[32] Kresse, G.; Hafner, J. *Ab Initio* Molecular Dynamics for Liquid Metals. *Phys. Rev. B* **1993**, *47*, 558–561.

[33] Kresse, G.; Hafner, J. *Ab Initio* Molecular Dynamics for Open-Shell Transition Metals. *Phys. Rev. B* **1993**, *48*, 13115–13118.

[34] Kresse, G.; Hafner, J. *Ab Initio* Molecular-Dynamics Simulation of the Liquid-Metal–amorphous-Sem iconductor Transition in Germanium. *Phys. Rev. B* **1994**, *49*, 14251–14269.